Chapter 4

Effect of Segment/Surface Shift on Motor Performance

4.1 Introduction

The performance of an electric machine (EM) primarily depends on the electromagnetic field distributions in the different parts of the machine. In the previous chapter, it is observed that the shifting of rotor segments or shifting of stator/rotor surfaces significantly reduces the torque ripple in DSSRM. However, the shift in the segment or surface will also deviate the flux distributions in core and air-gaps of the motor, which will affect the performance of the motor. In this chapter, the effect of segment and surface shift on the air-gap and core flux density is analyzed, and its influences on motor performances are discussed.

Rest of the Chapter is structured as follows: Section 4.2 investigate the distribution of flux density in the inner and outer air-gap of the motor and discusses the effect of segment and surface shift on the radial force of rotor segments. Section 4.3 investigate the effect of segment and surface shift on the behaviour of torque generation in commutation region and discusses the reason of torque ripple reduction. Section 4.4 analyzes the flux density in core and air-gaps as well as the aligned and unaligned inductances and discusses the influence of segment and surface shift on motor performance. Finally, Section 4.5 concludes the chapter.

4.2 Effect of segment/surface shift on radial force

The electromagnetic forces in an electric machine are the results of the interaction between normal and tangential components of air-gap flux density. The tangential and radial force densities in the air-gap can be expressed as [53]

$$f_r = \frac{1}{2\mu_0}(B_n^2 - B_t^2) \tag{4.1}$$

$$f_t = \frac{1}{2\mu_0} B_n B_t \tag{4.2}$$

where f_r and f_t are the radial and tangential force densities in the air-gap, respectively in N/m^2; B_n and B_t are the normal and tangential components of air-gap flux density, respectively in $Tesla$ and μ_0 is the permeability of free-space in H/m. Tangential force density (f_t) is responsible for generation of torque in the machine, while radial force density (f_r) leads to the generation of radial force and mechanical vibration in the machine.

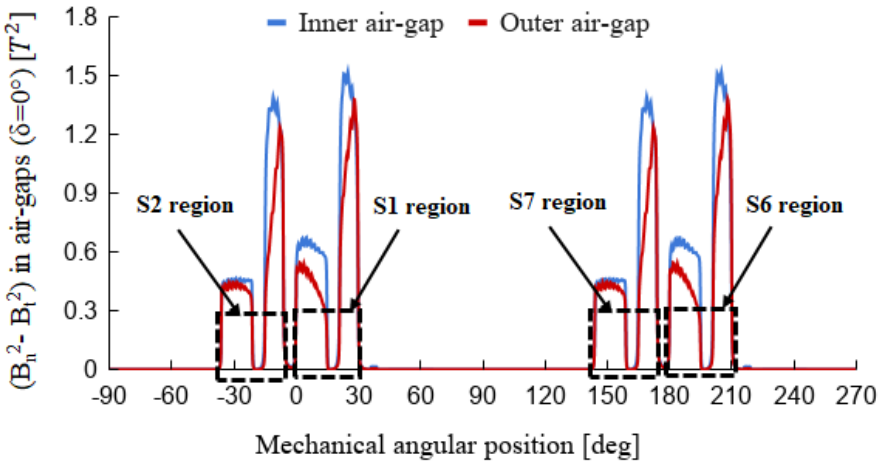

Figure 4.1: Plots of $(B_n^2 - B_t^2)$ for the inner and outer air-gaps of 12/10 pole DSSRM without segments shift ($\delta = 0°$) and 150° (elec.) rotor position.

4.2.1 Effect of segment shift on radial force

Rotor without segment shift (δ=0°)

It is seen in Eq. (4.1) that the radial force density is directly dependent on the value of $(B_n^2 - B_t^2)$ in the air-gap. Therefore, in this analysis, the values of $(B_n^2 - B_t^2)$ is calculated

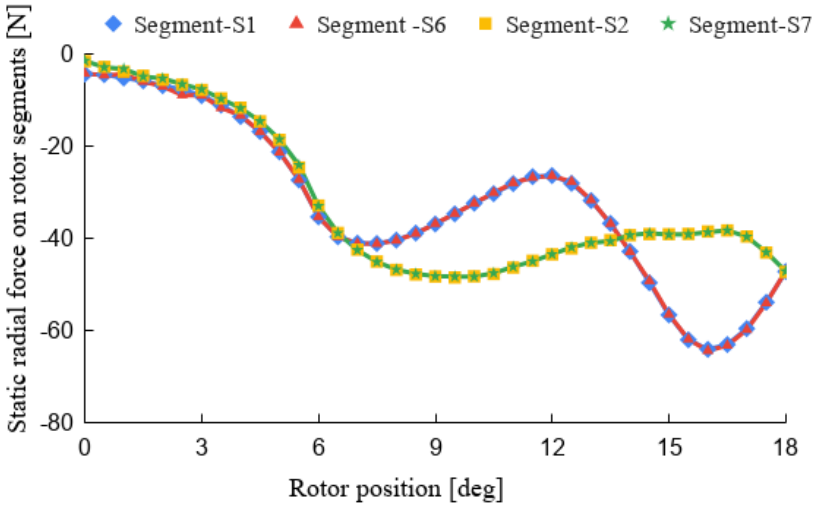

Figure 4.2: Static radial force on the rotor segments of 12/10 pole DSSRM without segments shift ($\delta = 0°$) and rated phase A current.

in the middle of inner and outer air-gaps of the DSSRM to investigate the radial force on the rotor segments. The plots of $(B_n^2 - B_t^2)$ are drawn for the inner and outer air-gaps between -90° to 270° mechanical position of motor (referred from Fig. 2.1 (a)). To calculate these values, the phase A is excited with the rated current of 26 A with the rotor at 150° (elec.) position.

Fig. 4.1 shows the plots of $(B_n^2 - B_t^2)$ for the inner and outer air-gaps of 12/10 pole DSSRM without segments shift (δ=0°). It is seen that for the excitation of phase A, the rotor segments S1, S2, S6 and S7 go into the magnetic influence of this phase. Therefore, the $(B_n^2 - B_t^2)$ has high peaks near the segments' region as shown in Fig. 4.1. The integration of $(B_n^2 - B_t^2)$ is carried out for the segments' region for both inner and outer air-gaps. The integral value of $(B_n^2 - B_t^2)$ for segment S1 region in the inner and outer air-gaps are 23.47 T^2 and 22.60 T^2, respectively. It is observed that this value is somehow higher for the inner air-gap than the outer one. Therefore, segment S1 has a resultant attractive radial force towards the inner stator side. The integral value of $(B_n^2 - B_t^2)$ is also calculated for the segment S6, which is diametrically opposite side of S1. It is observed that these values are nearly same as in the case of S1. Therefore, segment S6 also has the same attractive radial force towards the inner stator side. It is observed that S1 and S6 create an equal and opposite force on the rotor and make the balance condition on it. In the case of segments S2 and S7 (which is diametrically opposite side of

S2), these valuses are 19.75 T^2 and 19.41 T^2 for the inner and outer air-gap, respectively. Therefore, segments S2 and S7 also bear attractive radial force towards the inner stator side with same magnitude. This concludes that segments S2 and S7 also create equal and opposite force on the rotor. Because of these equal and opposite forces, the rotor has a balance condition and has the least vibrations for (δ=0°). Fig. 4.2 shows the static radial force working on segments S1, S2, S6 and S7 between 0°–18° rotor position with phase A excited with the rated current. The negative value represents that the force is in the direction of the inner stator side. It is seen that S1 and S6 have equal radial forces at all rotor positions. Likewise, S2 and S7 also have equal radial forces. The peak radial force on a rotor segment occurs near 16° rotor position and has a value of 64.9 N.

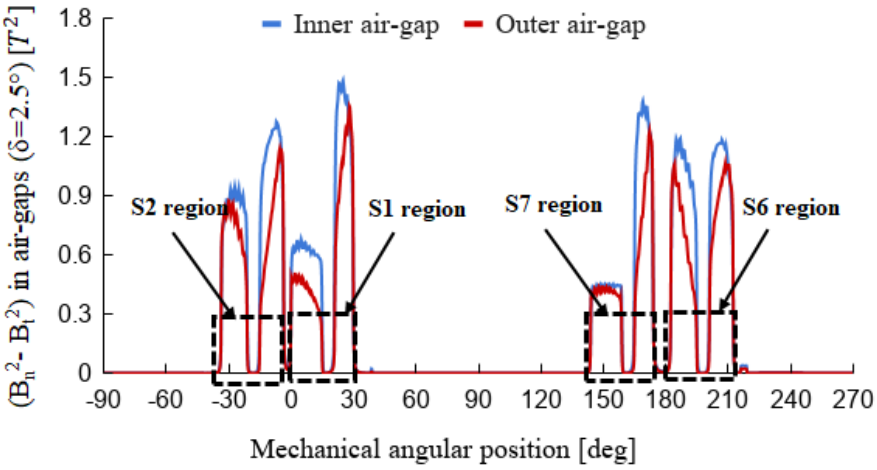

Figure 4.3: Plots of $(B_n^2 - B_t^2)$ in the inner and outer air-gaps of 12/10 pole DSSRM with $\delta = 2.5°$ and 150° (elec.) rotor position.

Rotor with segment shift (δ=2.5°)

In the case of rotor with the shifted segements, the angular separation between S1 and S2 reduces, whereas for S6 and S7 it increases. Fig. 4.3 shows the plots of $(B_n^2 - B_t^2)$ for the inner and outer air-gaps of the 12/10 pole DSSRM with segments shift ($\delta = 2.5°$). In this case, the difference between the integral values of $(B_n^2 - B_t^2)$ for the inner and outer air-gaps of segment S1 region is 1.35 T^2. Similarly, this value for S2, S6 and S7 are 0.68 T^2, 1.03 T^2 and 0.26 T^2, respectively. This observation concludes that all the

segments bear a resultant radial force towards the inner stator side. It is also seen that the difference values are not same for the opposite rotor segments. This value is higher for segment S1 as compared to opposite segment S6. Similarly, the difference value is higher for S2 as compared to S7. This observation concludes that S1 and S2, which have come closer after segments shift, have higher radial force than their opposite ones. Therefore, a small unbalance condition is created on the rotor. Fig. 4.4 shows the static radial force on the rotor segments between 0°–18° rotor position with the rated phase A current for the case of shifted segments ($\delta = 2.5°$). It is seen that the magnitude of the attractive radial forces on S1 and S6 are not same, similarly, it is not same for S2 and S7. Fig. 4.5 shows the dynamic unbalance force created on the rotor at the rated speed for shift angle $\delta = 2.5°$. The average value of this force is 33.9 N. The average value per cm of axial length is 3.94 N/cm. This small value will not cause any bending effect on the shaft, however, this force will lead some increase in mechanical vibrations in the motor.

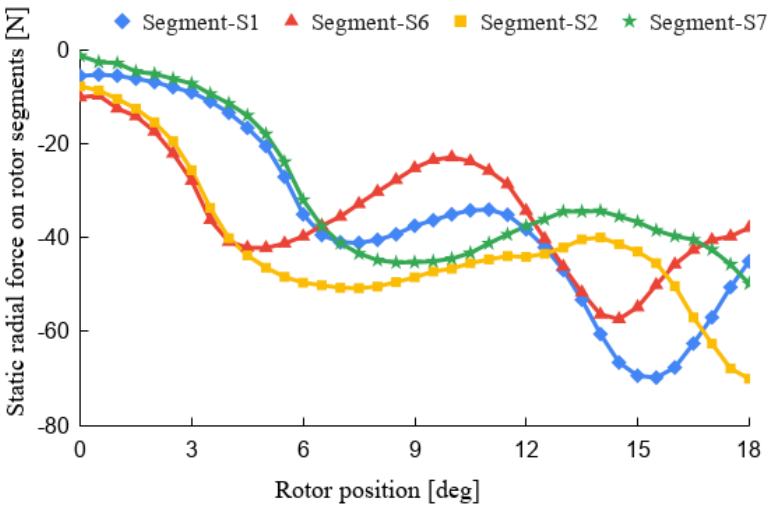

Figure 4.4: Static radial force on the rotor segments of 12/10 pole DSSRM with $\delta = 2.5°$ and rated phase A current.

The cause of the unbalanced magnetic force on the rotor of a 12/10 pole DSSRM is the unequal non-magnetic separation between the adjacent rotor segments at opposite sides of the rotor, as shown in Fig. 4.6 (a). This creates unequal radial force densities at opposite sides of the rotor which results in an inherent unbance condition on rotor. However, in the case of a 24/20 pole DSSRM, the number of stator and rotor poles becomes twice. Unlike 12/10 pole DSSRM, in 24/20 pole motor, the non-magnetic separation

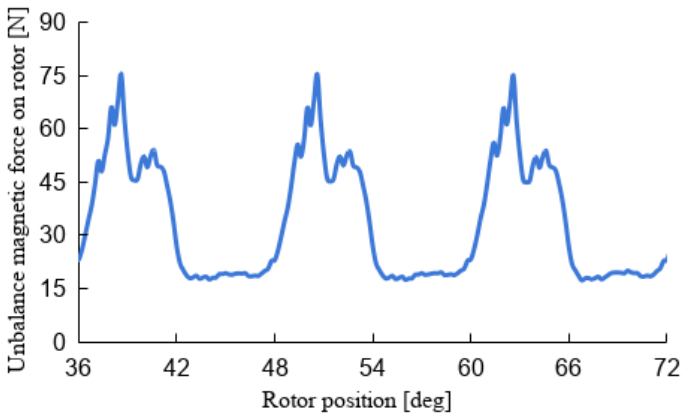

Figure 4.5: Dynamic force created on the rotor of 12/10 pole DSSRM with segments shift ($\delta = 2.5°$).

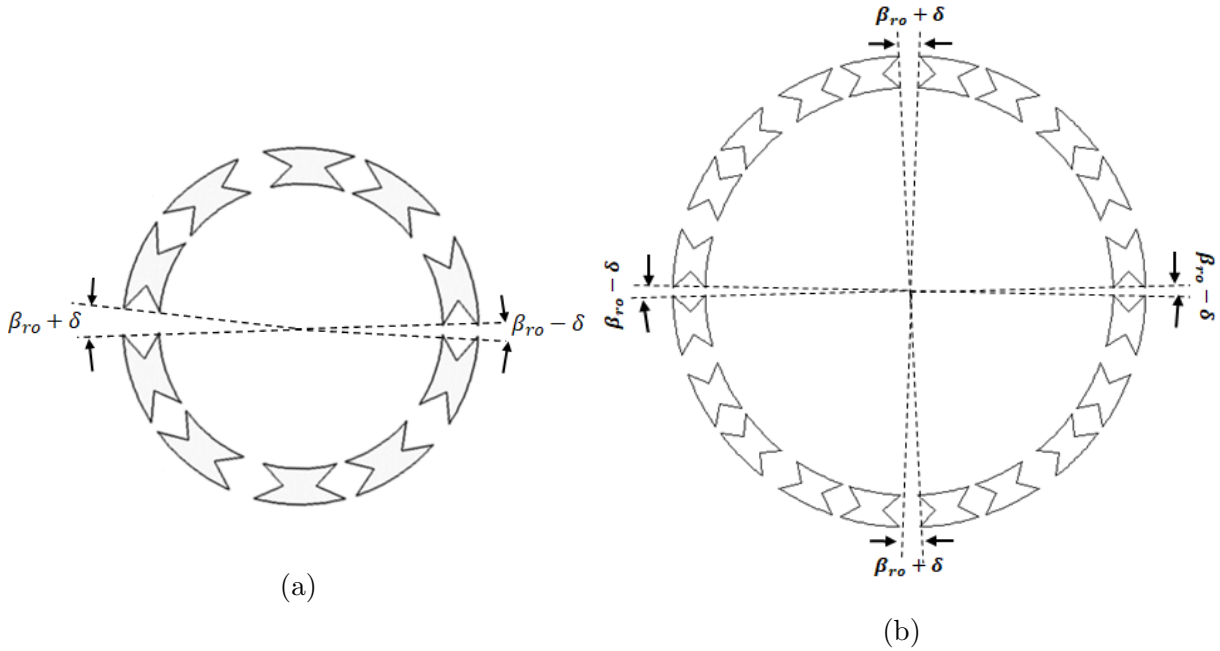

(a) (b)

Figure 4.6: Structure of the rotor of 12/10 and 24/20 pole DSSRM with shifted segments. (a) 12/10 pole DSSRM. (b) 24/20 pole DSSRM.

between adjacent rotor segments becomes equal at the opposite sides of the rotor, as shown in Fig. 4.6 (b). Because of this, the radial force densities in the air-gaps of opposite sides of the rotor become equal. This inherently omits the problem of unbalanced condition on the rotor and reduces the mechanical vibration in the motor. Fig. 4.7 shows the dynamic force on the rotor of a 24/20 pole DSSRM at the rated speed with shifted rotor segments which is discussed in Section 3.3 of the previous chapter. In this case, the average value of unbalanced force on the rotor is 0.5 N which is negligible.

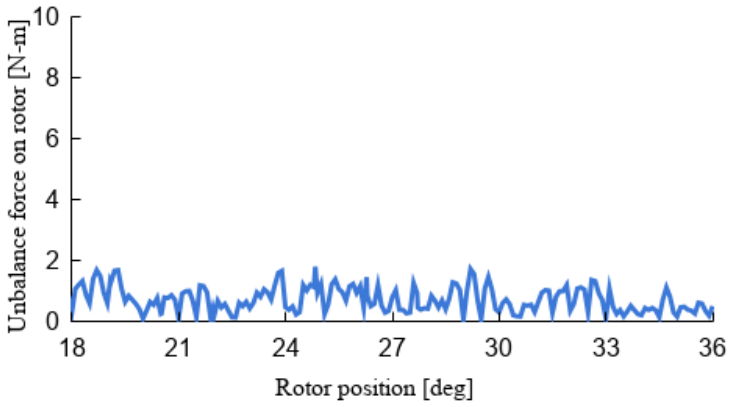

Figure 4.7: Dynamic force created on the rotor of 24/20 pole DSSRM with segments shift ($\delta = 1.5°$).

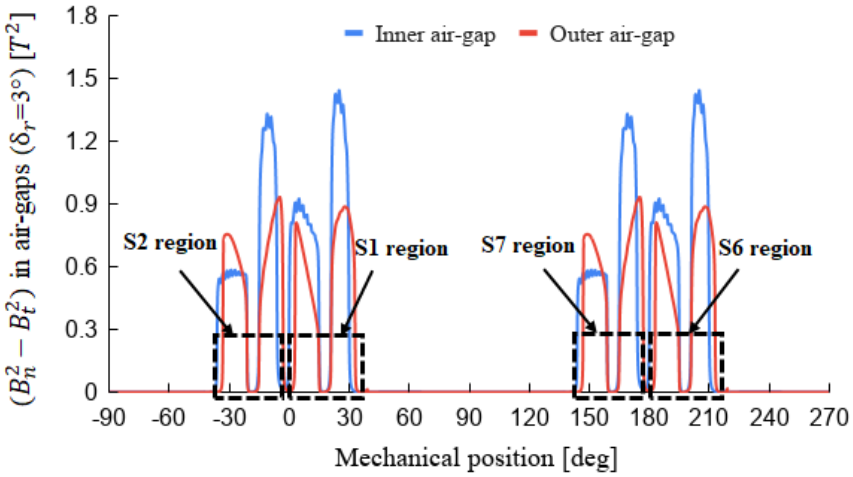

Figure 4.8: Plots of $(B_n^2 - B_t^2)$ in the inner and outer air-gaps of 12/10 pole DSSRM with the rotor's outer surface shift ($\delta_r = 3°$) and 150° (elec.) rotor position.

4.2.2 Effect of surface shift on radial force

Rotor surface shift

In the previous chapter, in Section 3.4, it is observed that shifting the rotor surfaces in the direction of rotation significantly reduces the torque ripple. It is also observed that the shifting of the rotor's outer surface is more effective in reducing the torque ripple than the inner or both surface shift. The minimum torque ripple occurs for 3° shift of

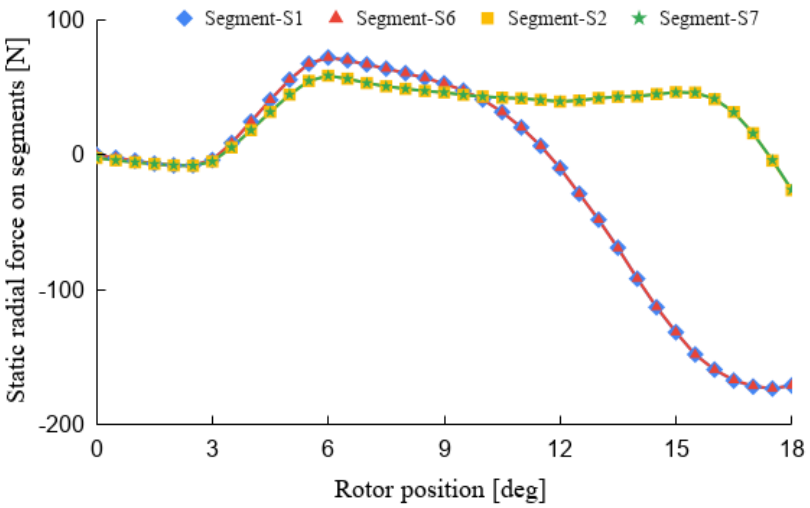

Figure 4.9: Static radial force on the rotor segments of 12/10 pole DSSRM with rotor's outer surface shift ($\delta_r = 3°$) and rated phase A current.

rotor's outer surface (δ_r=3°). The influence of this surface shift on the value of $(B_n^2 - B_t^2)$ in the air-gaps of DSSRM is investigated in this subsection. Fig. 4.8 shows the plots of $(B_n^2 - B_t^2)$ in the inner and outer air-gaps of 12/10 pole DSSRM with the rotor's outer surface shifted by 3°. The rotor position considered is 150° (elec.) position. For this case, the difference between the integral value of $(B_n^2 - B_t^2)$ for inner and outer air-gaps of segment S1 region is 3.25 T^2. This value for segment S6 region is also same. This shows that S1 and S6 have a resultant radial force of equal magnitude toward the inner stator direction. For segments S2 and S7, this difference value is -2.14 T^2. Therefore, S2 and S7 have equal magnitude of radial force towards the outer stator direction. A balanced condition occurs on the rotor because of equal and opposite forces on the diametrically opposite rotor segments. Fig. 4.9 shows the static radial force working on the rotor segments at different rotor positions with phase A excited with the rated current. It is seen that the diametrically opposite segments have equal magnitude of radial force at all rotor positions. The peak value of radial force on a rotor segment occurs near 17° rotor position. This value is 173.4 N which is significantly higher than the case without any shift. The reason for the higher value of peak radial force, in this case, is the shifting of only outer surface of the rotor, which increases the difference of $(B_n^2 - B_t^2)$ between inner and outer air-gaps and increases the resultant radial force on a rotor segment.

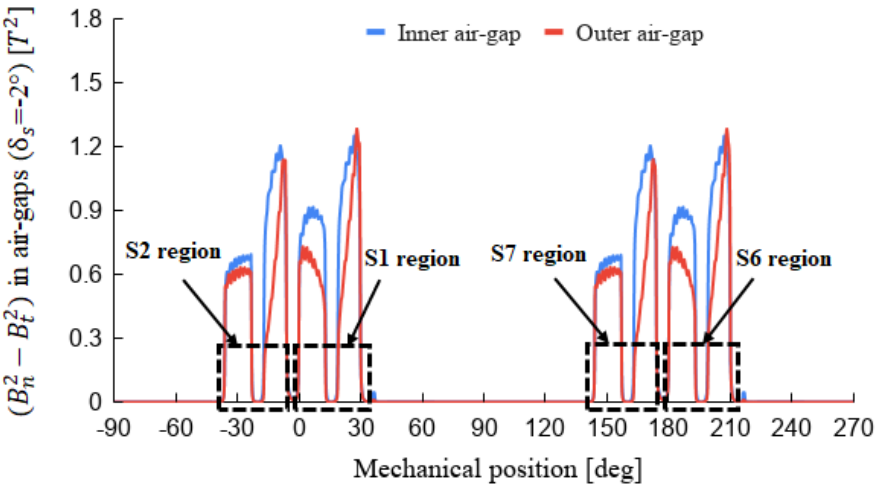

Figure 4.10: Plots of $(B_n^2 - B_t^2)$ in the inner and outer air-gaps of 12/10 pole DSSRM with both stator surface shift ($\delta_s = -2°$) and 150° (elec.) rotor position.

Stator surface shift

In the previous chapter, it is observed that shifting of both the stator surfaces opposite to the direction of rotation can effectively reduce the torque ripple in DSSRM. For the considered 12/10 pole motor, the shift angle $\delta_s = -2°$ provides a better compromise between the torque ripple reduction and average output torque. For this case, the torque ripple is reduced by 54.6%. The effect of this shift on the value of $(B_n^2 - B_t^2)$ in the air-gaps of DSSRM is investigated in this study. Fig. 4.10 shows the variation of $(B_n^2 - B_t^2)$ in the inner and outer air-gaps of the motor in the case when both stators' surface shifted by -2°. Phase A is excited with rated current with 150° (elec.) rotor position. In this case, the difference between the integral value of $(B_n^2 - B_t^2)$ for the inner and outer air-gaps of segment S1 region is 1.02 T^2, which is also same for segment S6 region. Similarly, this value for S2 and S7 is 0.83 T^2. This observation shows that all the rotor segments have a resultant radial force towards the inner stator direction. Moreover, the diametrically opposite rotor segments have equal and opposite force, which maintains the balance condition on rotor. Fig. 4.11 shows the static radial force on the rotor segments at different rotor positions with the rated value of phase A current. It can be seen that S1 and S6 have equal radial force; similarly, S2 and S7 also have equal radial force. The peak value of static radial force on a rotor segment occurs near 10° rotor position. This value is 74.3 N which is 14.5% greater than the case of without any surface shift.

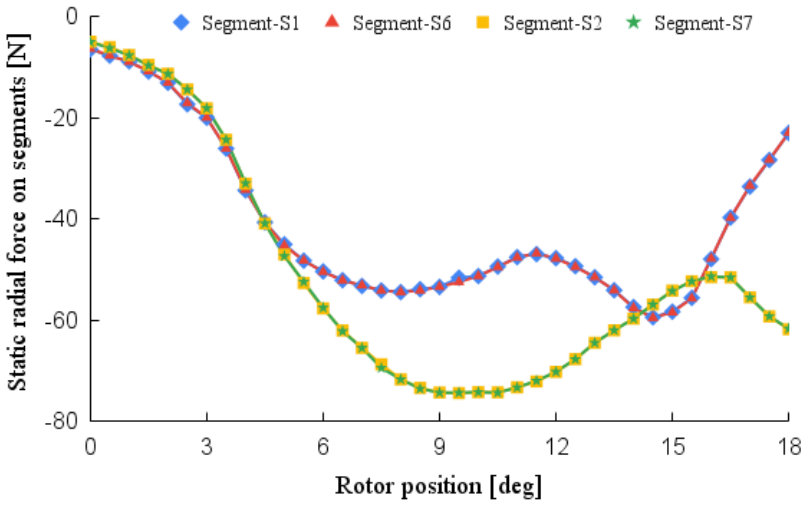

Figure 4.11: Static radial force on the rotor segments of 12/10 pole DSSRM with both stator surface shift ($\delta_s = -2°$) and rated phase A current.

Stator-rotor surface shift

It is observed in Section 3.4 of the previous chapter that the simultaneous shift of stator and rotor surfaces can effectively reduce the torque ripple in DSSRM. In the case of 12/10 pole DSSRM, the total shift of 2° provides the minimum value of torque ripple. The effect of this shift on the value of $(B_n^2 - B_t^2)$ in the air-gaps of DSSRM is investigated here. Fig. 4.12 shows the variation of $(B_n^2 - B_t^2)$ in the inner and outer air-gaps of the DSSRM with the stator-rotor surface shift (δ_t=2°). Phase A is excited with the rated current with 150° (elec.) rotor position. In this case, the difference between the integral value of $(B_n^2 - B_t^2)$ in the inner and outer air-gaps for segment S1 (and S6) region is 1.50 T^2. Similarly, this value for S2 and S7 regions is 0.37 T^2. Therefore, these segments have a resultant radial force towards the inner stator direction. The diametrically opposite rotor segments have equal and opposite forces; consequently, they make a balance condition on the rotor. Fig. 4.13 shows the static radial force on the rotor segments between 0° to 18° rotor position with phase A excited with the rated current. It is seen that S1 and S6 have equal radial force at each rotor position. Similarly, S2 and S7 also have equal radial force. The peak value of radial force on a rotor segment occurs near 16° rotor position. The peak radial force, in this case, is 80.7 N, which is 24.3% greather than the case without any shift.

Table 4.1 enlists the comparative data in the view of peak radial force on a rotor

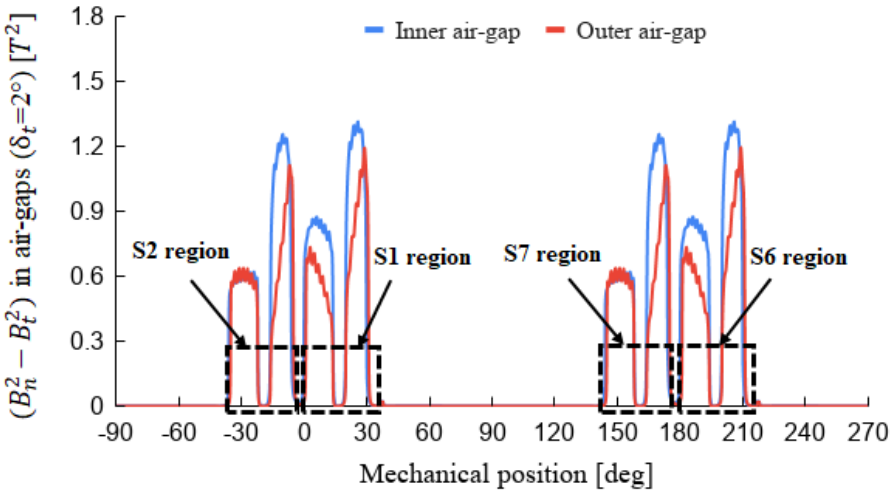

Figure 4.12: Plots of $(B_n^2 - B_t^2)$ in the inner and outer air-gaps of 12/10 pole DSSRM with stator-rotor surface shift ($\delta_t = 2°$) and 150° (elec.) rotor position.

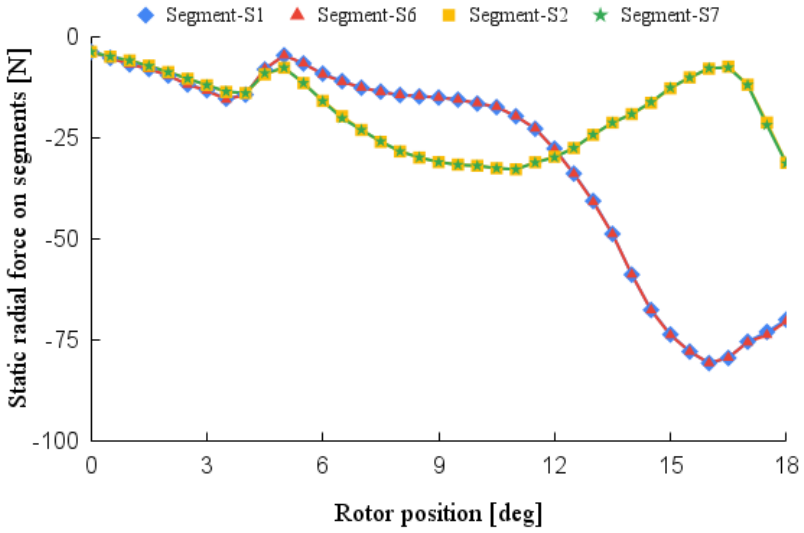

Figure 4.13: Static radial force on the rotor segments of 12/10 pole DSSRM with stator-rotor surface shift ($\delta_t = 2°$) and rated phase A current.

segment for the different surface shift. It is observed that shifting both the stator surfaces results in a lesser increase in radial force and vibrations as compared to other surface shift.

Table 4.1: Comparison of radial force on a rotor segment for different surface shift.

Parameter	No shift	Outer rotor surface shift	Both stator surface shift	Stator-rotor surface shift
Peak radial force on a segment	64.9 N	173.4 N	74.2 N	80.7 N
% increase in peak radial force	–	167.2%	14.5%	24.3%

4.3 Effect of segment/surface shift on tangential force

As seen in Eq. (4.2), the tangential force density and output torque is directly dependent on the value of $(B_n B_t)$ in the air-gap. Therefore, in this analysis, the values of $(B_n B_t)$ is calculated in the middle of inner and outer air-gaps of the DSSRM to investigate the behaviour of output torque in the motor. The plot of $(B_n B_t)$ in inner air-gap of the 12/10 pole DSSRM is shown in Fig. 4.14 (a), without and with rotor segments shift between -90° to 270° mechanical position of motor. This value is shown in Fig. 4.14 (b) for outer air-gap. The rotor position considered is 15° (mech.), just after the start of the commutation of phase A. With the excitation of phase B, the segment S3, S4, S8 and S9 go into its magnetic infuence. It is seen in figures that the values of $(B_n B_t)$ in the inner and outer air-gaps, near the segments S4 and S8 region, are increased in the case of shifted segments. Therefore, more tangential forces are exerted on these segments which increase the torque generation of the motor in the commutation region. Because of this, the torque dip and subsequently, the torque ripple reduces in this region.

Like segments shift, shifting of stator and rotor surfaces also increase the tangential force density and output torque in the commutation region. Fig. 4.15 shows the plots of $(B_n B_t)$ in the inner and outer air-gaps of 12/10 pole DSSRM for the case without and with stator surface shift. The rotor position considered is 15° (mech) just after the commutation of phase A. It is seen in figures that the values of $(B_n B_t)$ in the inner and outer air-gaps, near the segments S3, S4 S8 and S9 regions, are increased in the case of stators surface shift. Therefore, more tangential forces are exerted on these segments, which increase the torque generation of the motor in the commutation region and reduces the torque ripple.

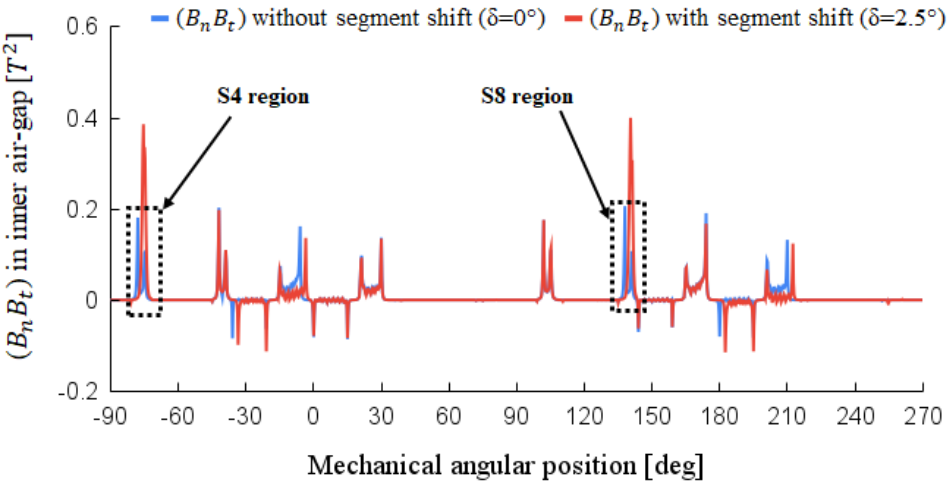

(a)

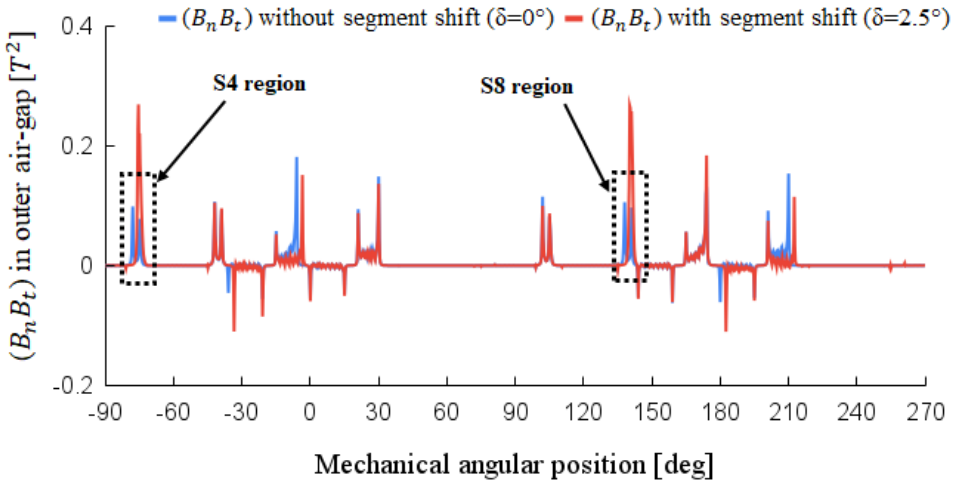

(b)

Figure 4.14: Plots of (B_nB_t) in inner and outer air-gaps of 12/10 pole DSSRM without and with rotor segment shift just after the start of the commutation of phase A. (a) B_nB_t in inner air-gap. (b) B_nB_t in outer air-gap.

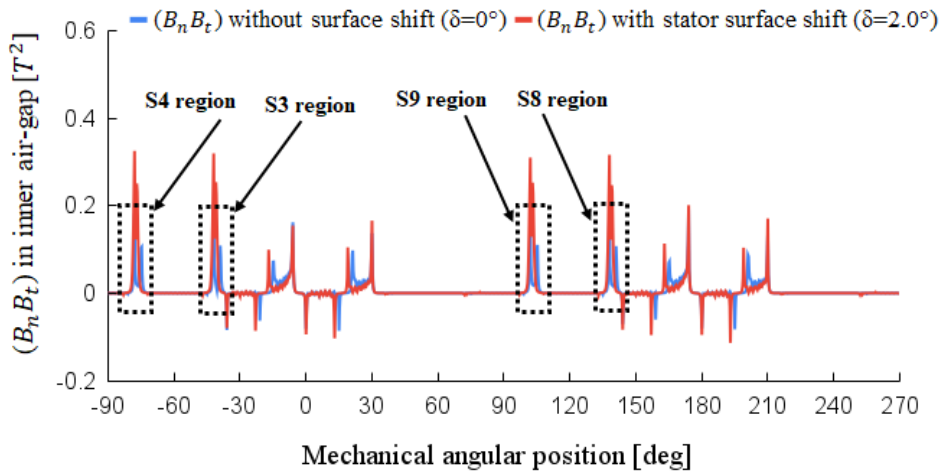

(a)

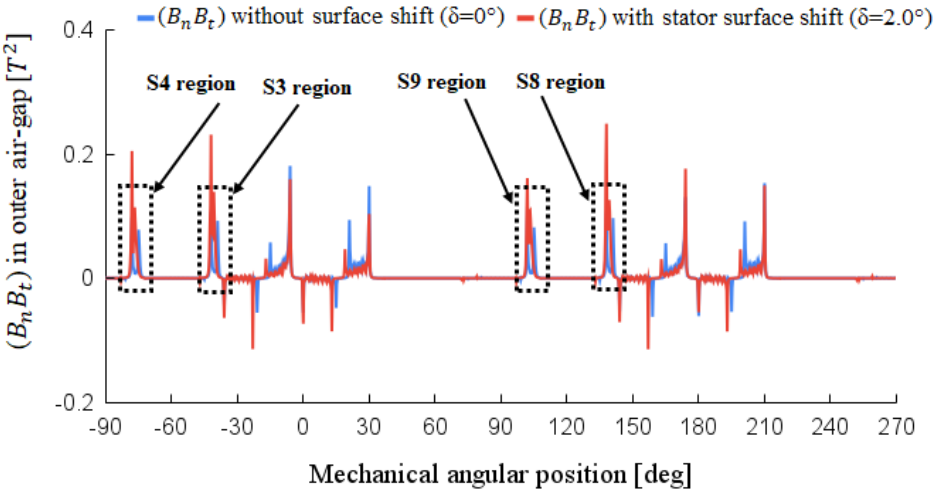

(b)

Figure 4.15: Plots of (B_nB_t) in inner and outer air-gaps of 12/10 pole DSSRM without and with stator surface shift just after the start of the commutation of phase A. (a) B_nB_t in inner air-gap. (b) B_nB_t in outer air-gap.

4.4 Effect on motor performance

4.4.1 Effect of segment shift on motor performance

In this subsection, the effect of the segments shift on the flux distributions in the rotor segments as well as in the air-gaps are analyzed and their influences are discussed. Fig. 4.16 (a) shows the variation in the maximum flux density occurring in the rotor segments with the segment shift angle (δ). The shifting of the rotor segments results in some of

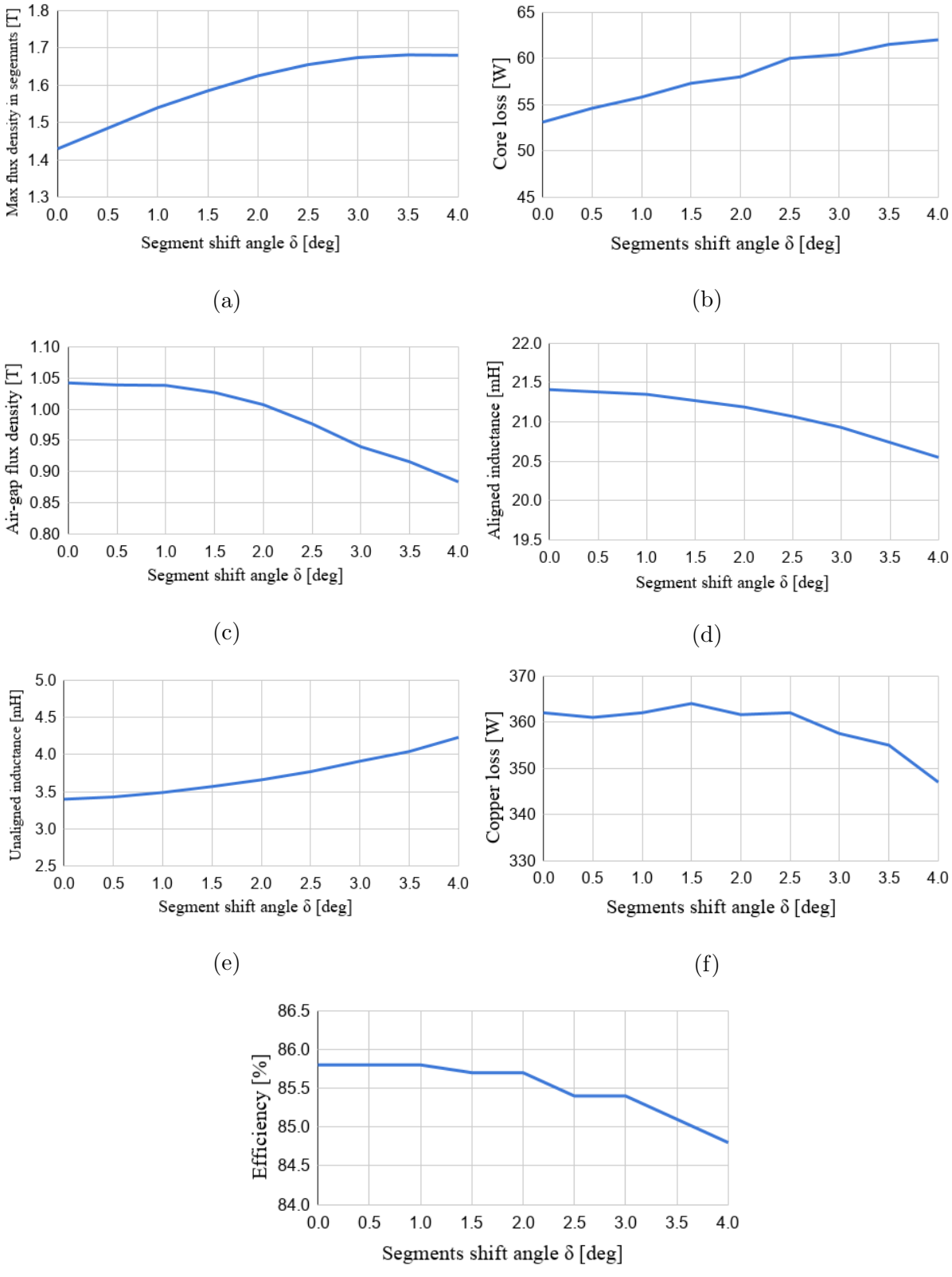

Figure 4.16: Variation in the parameters of DSSRM with segments shift angle (δ). (a) Flux density in segments. (b) Core loss. (c) Air-gap flux density. (d) Aligned inductance. (e) Unaligned inductance. (f) Copper loss. (g) Efficiency.

the adjacent rotor segments coming closer, therefore, the flux increases in these segments. This increases the maximum flux density in the rotor segments. As shown in the figure, the maximum flux density in the segments is 1.43 T for $\delta = 0^{\circ}$ which increases to 1.65 T for $\delta = 2.5^{\circ}$. With further increase in δ, the saturation effect becomes more significant and flux density becomes nearly constant in the rotor segments. With the increase in flux density, the core loss increases. Fig. 4.16 (b) shows the variation in core loss of motor with δ. The core loss increases with the increase in δ because of the increase in the flux density in rotor segments.

Fig. 4.16 (c) shows the variation in air-gap flux density with δ. The air-gap flux density shown is the average value of inner and outer air-gaps. With the increase in δ, the air-gap flux density decreases because of the increase in leakage flux. It is seen that the decrease in air-gap flux density is more rapid for δ greater than 2°. Eq. (2.4) shows that the aligned inductance is directly dependent on the air-gap flux density; therefore, it also decreases with the increase in δ, which is shown in Fig. 4.16 (d). Fig. 4.16 (e) shows the variation in the unaligned inductance with δ. It is seen that with the increase in δ, the unaligned inductance increases. This is because of the increase in the leakage flux in the rotor segments near the unaligned condition. As given in Eq. (2.8), the decrease in air-gap flux density and aligned inductance, and the increase in unaligned inductance will result in the reduction of the output torque for the higher value of δ. In Fig. 3.6 (b), it can be observed that the output torque reduces more rapidly for δ above 2.5°. The increase in unaligned inductance further reduces the rate of increase of the phase currents. Therefore, the phase current and the copper loss starts decreasing rapidly above the value of $\delta = 2.5^{\circ}$, which is shown in Fig. 4.16 (f). However, the decrease in phase current will further reduce the output torque and power.

It is observed that for the higher values of δ, above 2.5°, the decrease in air-gap flux density and aligned inductance; and increase in unaligned inductance is significant which will reduce the phase current and output torque and power. The reduction in torque and power will lead to the reduction in efficiency which is shown in Fig. 4.16 (g).

4.4.2 Effect of surface shift on motor performance

In the previous chapter, it has been observed that shifting of the stator and rotor surfaces significantly reduces the torque ripple in DSSRM. It also divulges that the shifting of both

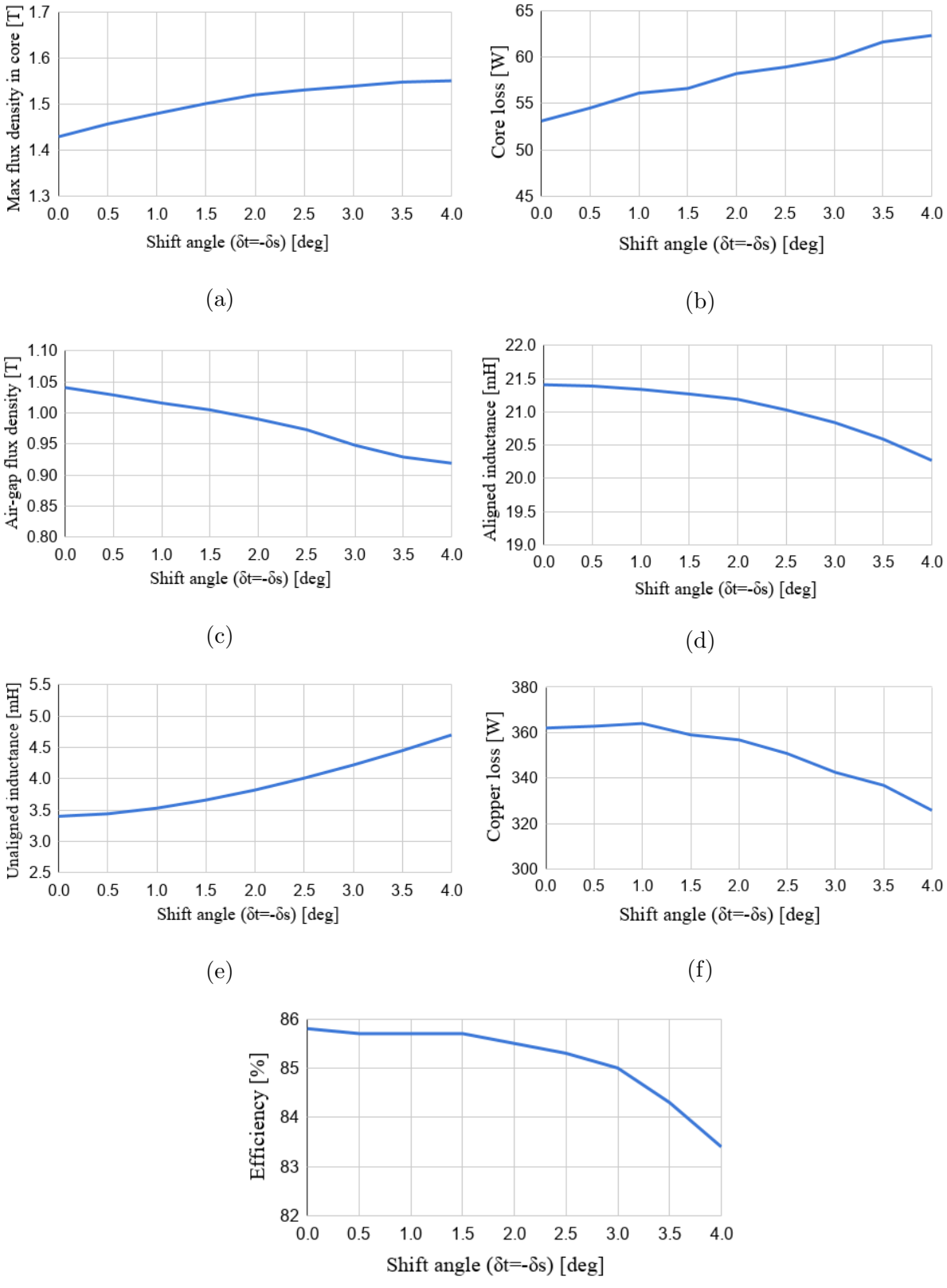

Figure 4.17: Variation in the parameters of DSSRM with stator surface shift. (a) Flux density in segments. (b) Core loss. (c) Air-gap flux density. (d) Aligned inductance. (e) Unaligned inductance. (f) Copper loss. (g) Efficiency.

stator surfaces is dominant in reducing the torque ripple compared to other shifts. The minimum torque ripple is observed when both stators' surfaces are shifted by 2° (δ_t=2°). In this subsection, the effect of this shift on the flux density variation and motor performance is discussed. Fig. 4.17 (a) represents the variation of the maximum flux density in the iron core with the variation of δ_t. Core flux density increases linearly with the increase in shift angle until the value of δ_t=2°. However, the rate of flux density increment reduces because of the saturation effect for the further increase in δ_t. Fig. 4.17 (b) shows the variation of core loss with the variation of δ_t. The core loss increases with the increase in δ_t because of the increase in core flux density.

Fig. 4.17 (c) represents the variation of the air-gap flux density with δ_t. The air-gap flux density reduces with the increase in δ_t. Because of the decrease in air-gap flux density, the aligned inductance also decreases, which is shown in Fig. 4.17 (d). Fig. 4.17 (e) shows the variation of unaligned inductance with δ_t. The leakage flux density increases in the motor, increasing δ_t, which subsequently increases the unaligned inductance. The decrease in air-gap flux density, aligned inductance and increase in unaligned inductance reduces the output torque for the higher value of δ_t.

The increase in unaligned inductance further reduces the rate of the rise of the phase current. Fig. 4.17 (f) shows the variation in copper loss with δ_t. For a higher value of δ_t, the phase current reduces, which further reduces the motor's output torque, copper loss and efficiency. Fig. 4.17 (g) represent the variation of efficiency of the motor with δ_t. The reduction in output torque and efficiency for δ_t greater than 2° is significant.

4.5 Conclusions

In this chapter, the effect of segment and surface shift on the performance of the DSSRM has been introduced. The effect of segment and surface shift on the radial force of rotor segments has been explored with the help of the normal and tangential components of the inner and outer air-gap flux densities. Shifting the rotor segments of a 12/10 pole motor introduces a small unbalance force on the rotor because of the unequal radial force densities in the air-gaps of the opposite sides of the rotor. However, this unbalance condition is inherently omitted in the case of 24/20 pole motor. Shifting of stator and rotor surfaces does not result in unbalancing condition on the rotor. Moreover, the segment

and surface shift increases the peak value of radial force on a rotor segment.

The effect of segment and surface shift on the output torque in the commutaion region is studied. It is observed that the value of $(B_n B_t)$ increases in this region, in the case of segment or surface shift. This increases the output torque and reduces torque ripple in this region.

The effects of segment and surface shift on the core and air-gap flux densities as well as aligned and unaligned inductances, are discussed. For a higher degree of shift angle, these values change considerably, which reduces the output torque and efficiency of the motor.

In the next chapter, the design concepts of a new DSSRM have been explored, which has a significantly low torque ripple in higher speed region.